EUROPEAN ORGANIZATION FOR NUCLEAR RESEARCH
CERN — AB DEPARTMENT

CERN-AB-2006-023 BI

ALTERNATIVE TECHNIQUES FOR BEAM HALO MEASUREMENTS

C.P. Welsch, E. Bravin, B. Burel, T. Lefèvre
CERN, Geneva, Switzerland
T. Chapman, M.J. Pilon
Thermo Electron Corporation, Liverpool, NY USA

Abstract

In future high intensity, high energy accelerators it must be ensured that particle losses are minimized, as activation of the vacuum chambers or other components makes maintenance and upgrade work time consuming and costly. It is imperative to have a clear understanding of the mechanisms that can lead to halo formation and to have the possibility to test available theoretical models with an adequate experimental setup.

Measurements based on **o**ptical **t**ransition **r**adiation (OTR) are a well-established technique for measurements of the transverse beam profile. However, in order to be suitable for halo measurements as well, the dynamic range of the final image acquisition system needs to be high, being able to cover at least five orders of magnitude in intensity changes.

Here, the performance of a standard acquisition system as it is used in the **C**LIC **t**est **f**acility (CTF3) is compared to a step-by-step measurement with a small movable photo multiplier tube and an innovative camera system based on **c**harge **i**njection **d**evice (CID) technology. Special emphasis is given on a description of the characteristics of the latter system.

Published in MEASUREMENT SCIENCE AND TECHNOLOGY journal ref. Meas. Sci. Technol. ***17*** *(2006) 2035–2040*

Geneva, Switzerland
June, 2006

ALTERNATIVE TECHNIQUES FOR BEAM HALO MEASUREMENTS

C.P. Welsch, E. Bravin, B. Burel, T. Lefèvre
CERN, Geneva, Switzerland
T. Chapman, M.J. Pilon
Thermo Electron Corporation, Liverpool, NY USA

Abstract

In future high intensity, high energy accelerators it must be ensured that particle losses are minimized, as activation of the vacuum chambers or other components makes maintenance and upgrade work time consuming and costly. It is imperative to have a clear understanding of the mechanisms that can lead to halo formation and to have the possibility to test available theoretical models with an adequate experimental setup.

Measurements based on **o**ptical **t**ransition **r**adiation (OTR) are a well-established technique for measurements of the transverse beam profile. However, in order to be suitable for halo measurements as well, the dynamic range of the final image acquisition system needs to be high, being able to cover at least five orders of magnitude in intensity changes.

Here, the performance of a standard acquisition system as it is used in the **C**LIC **t**est **f**acility (CTF3) is compared to a step-by-step measurement with a small movable photo multiplier tube and an innovative camera system based on **c**harge **i**njection **d**evice (CID) technology. Special emphasis is given on a description of the characteristics of the latter system.

INTRODUCTION

For a future linear collider, it will be of central importance to have a detailed understanding of beam halo formation, since beam losses in high intensity machines will cause severe activation of the surrounding vacuum chambers and thus complicate maintenance and increase costs. Several mechanisms can lead to the formation of a beam halo including machine mismatch, beam dispersion and scattering effects [1]. Measurements done in proton machines [2,3] confirm, to a large extent, the validity of the particle core model [4,5,6].

On the other hand, limited experience on halo formation in intense electron beams is available on the international scene, and besides the clear need for corresponding models, beam diagnostic techniques need to be developed that allow experimental verification.

One possible approach towards high dynamic range measurements is the exploitation of OTR created by the electron beam when passing through a thin screen introduced into the beam line. This kind of radiation guarantees a fast time response and very good linearity with the beam signal over a wide intensity range. The number of OTR photons created per electron in the optical wavelength interval between λ_a and λ_b at an energy γ is given by [7]

$$N_{OTR} = \frac{2\alpha}{\pi} \ln\left(\frac{\lambda_b}{\lambda_a}\right)\left[\ln(2\gamma) - 1/2\right] \tag{1}$$

where the fine structure constant $\alpha = e^2/(\hbar c) \approx 1/137$ was used.

Taking into account the total number of 10^{10} electrons per bunch with an energy of up to 150 MeV in CTF3, a possible halo monitor needs to cover a dynamic range of at least 10^5 to allow the verification of theoretical models.

LIGHT SOURCE AND CCD MEASUREMENTS

Due to the high radiation level in CTF3 and associated problems, preliminary measurements with different acquisition techniques were carried out in an optical lab. The light distribution from the electron beam was simulated by means of an Opto-Electronics PLS20 Pulsed Diode Laser. This source guarantees stable operating conditions, good reproducibility of the measurements and allowed the simulation of divergent light similar to what would be created by OTR from the electron beam. It thus serves as a test system for any kind of diagnostic technique using light created by an accelerated ion or electron beam. The Gaussian shape of the laser corresponds to the (idealized) beam in an accelerator and provides a dynamic range of ~10^7.

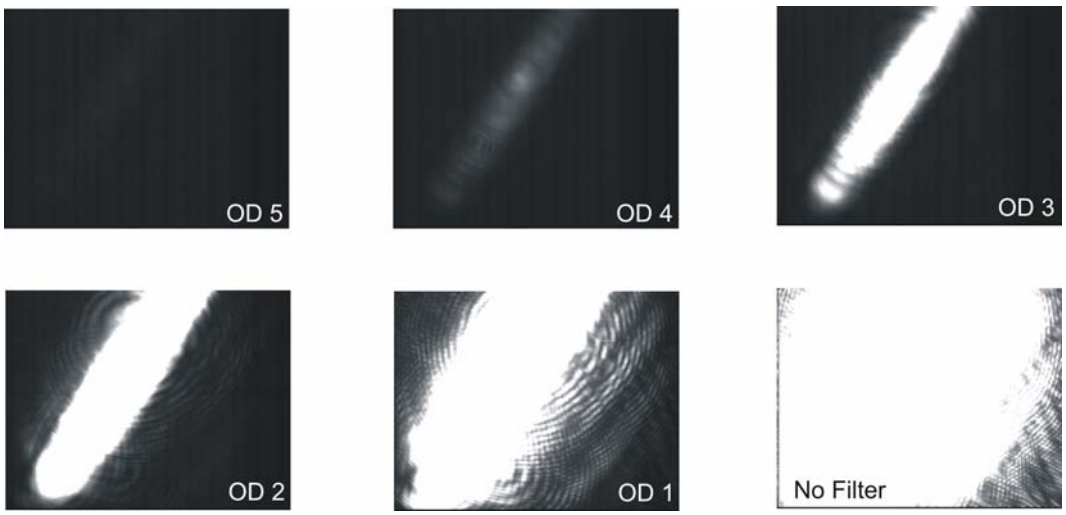

Figure 1: Laser profile as measured with the CCD camera in combination with five different optical density filters

This laser was used to benchmark the present camera used at CTF3, a Sanyo VCB-3385P, with a pixel size of 6.5 μm *(h)* x 6.25 μm *(v)*, against two other possible techniques: A step-by-step measurement with a small photomultiplier tube and the SpectraCAM™84 system based on CID technology.

The light source was placed at a distance of 22 cm from either of the detection systems, and directly illuminated the respective detectors. As can be seen in Figure 1, the light level from the laser was high enough to saturate almost the entire CCD chip when no optical density filter was applied. Therefore, filters from optical density (OD) 1 to OD5 were placed in between the laser and the camera. Image acquisition was then done by an 8-bit frame grabber card.

From these images, the intensity distribution along the main axes of the laser point can be derived as shown in Figure 2. For each measurement, the inherent pixel noise was determined and subtracted from the original data before normalization. Note that blooming effects are minimal with this type of CCD camera, and saturation of pixels results from photons impinging on the actual pixel site as opposed to charge spill over from adjacent pixel sites. The OD4 filter provided the best data since it limited pixel saturation to the very centre of the CCD and provided a reasonable signal to noise ratio of about 100:1, and thus serves as the basis for the later comparison of the different detection techniques. A Gaussian fit to this specific intensity distribution is shown in Figure 3.

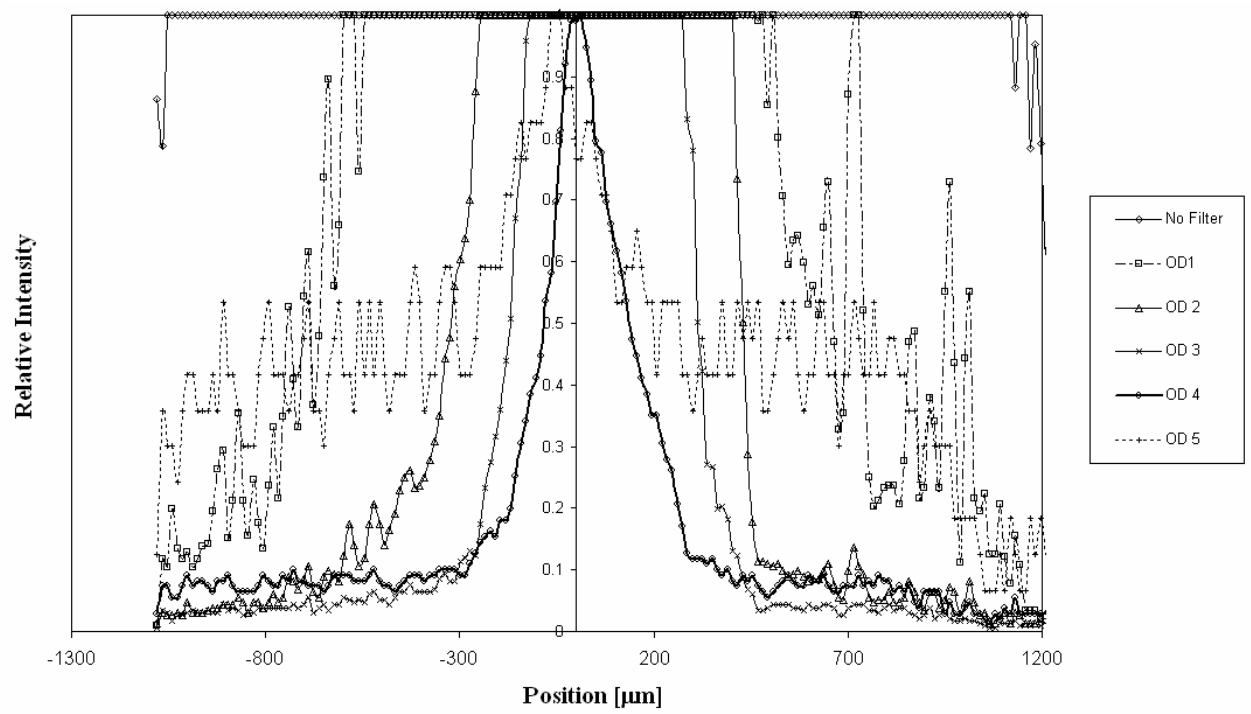

Figure 2: Measured intensity distribution of the pulsed laser with different density filters

Possible improvements on measurements with such a standard CCD camera system might be realized by using a *core masking technique* as it was already tested at CTF3 in the past [8], or by using *micro mirror arrays* [9] to exclude the central part of the light cone.

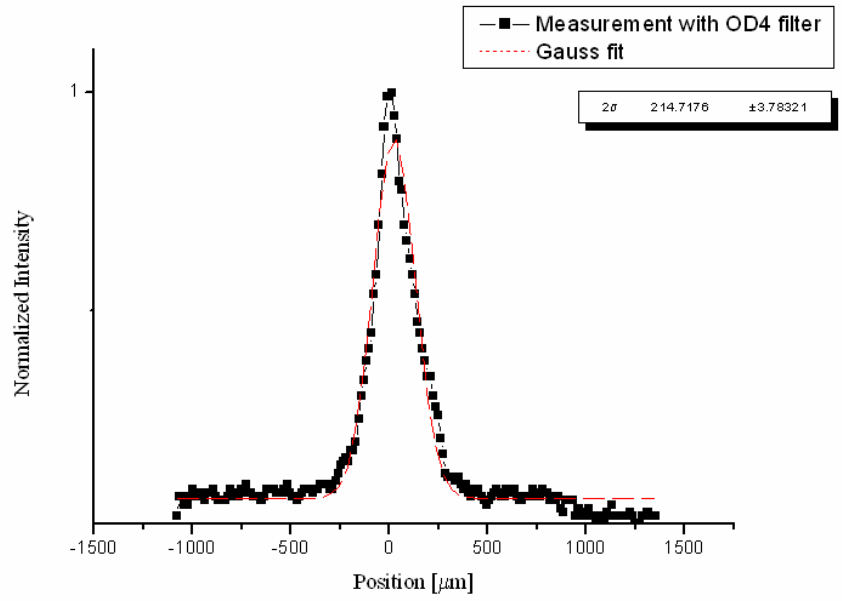

Figure 3: Normalized intensity as a function of position for the case of the OD4 filter

This CCD camera system has been employed in CTF3 because it provides a cheap and reliable image acquisition system that is easily integrated into the existing control system. It is important to note that the camera was not selected to provide for high dynamic range measurements or beam halo measurements.

THE CID CAMERA

Charge injection devices (CIDs) are in the class of solid-state imaging electronics called charge transfer devices (CTDs). When a photon penetrates the surface of the device, it induces the creation of an electron-hole pair, and the resulting photon-generated charge is integrated into a regularly spaced, two-dimensional array of electronic storage cells called 'pixels.' The entire array or imaging sensor is referred to as a 'charge transfer device' because of the mechanisms used to systematically read the photon-generated charge from the pixel sites. The charge coupled device (CCD) employs an inter-cell charge transfer readout mechanism whereby the charge packets are physically transferred in a bucket-brigade fashion from pixel to pixel, then on to a parallel register, and finally to a single readout amplifier. This inter-cell charge transfer readout process is destructive to the photon-generated charge. Conversely, the CID employs an intra-cell charge transfer mechanism to readout pixels whereby the charge is transferred from one electrode (the 'drive' or 'row' electrode) to the other electrode (the 'sense' or 'column' electrode) entirely **within** the pixel site. The voltage change on the 'sense' electrode that is induced by this movement of charge is then measured. The resulting voltage change is proportional to the amount of photon-generated charge within the pixel site, and this intra-cell charge transfer readout mechanism is non-destructive to the photon-generated charge.

Each CID pixel consists of a p-doped silicon substrate on top of which an n-type epitaxial layer is grown. The pixels are defined by a checker board type field oxide pattern that is grown across the surface, before the row (drive) and column (sense) electrodes are applied in thin strips of poly-silicon. The intersection region of these two electrodes then defines the active area of each single pixel. The pixel size of the SpectraCAM™84 used in our measurements is 27 μm x 27 μm. The CID is adequately responsive in a wavelength range extending from 165 nm to 1100 nm, and thus has broader applicability than that of most front-illuminated CCD sensors. The number of photon-generated electrons (or holes) that can be stored in each CID pixel site before saturation (i.e., the full well capacity) is around 5.0×10^5 electrons.

Although it was invented more than two decades ago by G. Michon at General Electric [10], and although it offers a number of interesting advantages in direct comparison to CCD cameras, CID technology is still not widely used in the field of particle accelerators. The "charge injection device (CID)" derives its name from its unique ability to clear individual pixel sites of photon-generated charge by *injecting* the charge directly into the substrate. The main features of this imager technology are its distinctive readout capabilities including inherent resistance to ionizing radiation, inherent resistance to charge blooming, true random pixel addressability, non-destructive pixel readout (NDRO), and on-sensor collective pixel readout and clear. The on-sensor collective read feature allows the data acquisition routines to select contiguous pixel regions (e.g., a 3 by 3 pixel region) and interrogate those pixels with a single reading that is the electronic average of the signals on those pixels, thereby improving both readout speed and signal-to-noise ratio. This collective read feature is analogous to the 'binning' that can be performed with certain CCD camera systems. However, unlike the CCD where the charge packets from the individual pixels are physically combined into a single larger charge packet, the CID collective read feature preserves the spatial integrity of the photon-generated charge in the pixels and the read process is non-destructive to that charge. The CID architecture also allows for the clearing of photon-generated charge from contiguous pixel regions with a single 'inject' pulse.

Each pixel on the CID imager is individually addressable and allows for random access non-destructive pixel readout. This feature is illustrated in Figure 4. During image acquisition, the photon-generated charge is typically stored under the row (or drive) electrode (see stage 1). In order to determine the level of accumulated charge, the column (or sense) electrode is allowed to float, and the 1st voltage sample is taken on the electrode (see stage 2). Next, the row (or drive) electrode voltage is collapsed thereby causing the photon-generated charge to transfer to the column (or sense) electrode. At this point, the 2nd voltage sample is acquired (see stage 3).

The voltage difference between the 2nd voltage sample and the 1st voltage sample is proportional to the amount of photon-generated charge at the pixel site. At this point, the column and row electrodes may be returned to their original bias conditions allowing for the continued integration of photon-generated charge (see stage 1), or alternatively, the voltages on both electrodes can be collapsed thereby causing the pixel to be cleared of charge (see stage 4).

As demonstrated in Figure 4, photon-generated charge may be transferred within each individually addressable pixel for readout without actually destroying the charge – a clear advantage in comparison to any other camera technique.

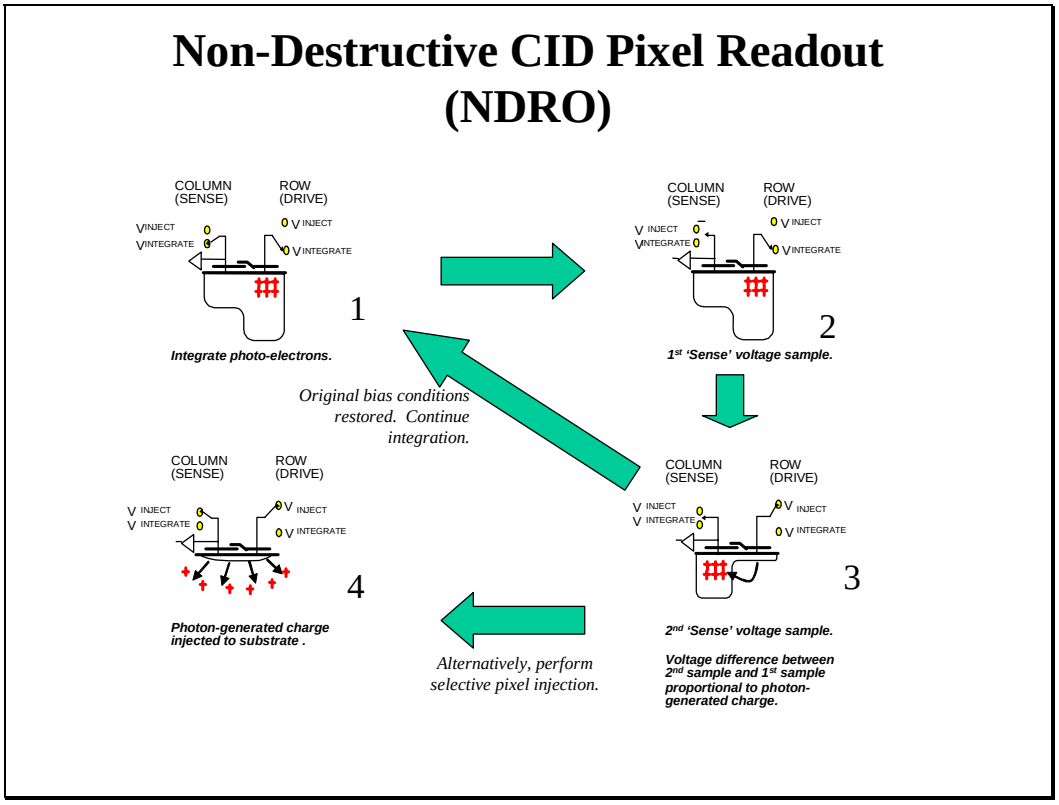

Figure 4: CID Non-Destructive Readout (NDRO) and Selective Pixel Clear.

The SpectraCAM™84 camera firmware features several image acquisition modes: The *Fixed Time* exposure acquisition mode is analogous to an exposure acquired on a standard CCD where the user enters a desired exposure time and the CID is simply exposed for that period of time; The *Time Resolved* mode allows for the acquisition of signal (i.e., number of photons incident on user-defined regions of interest) as a function of time, and thus provides an ideal built-in tool for the initial optimization of the light intensity; and finally, the ***R****andom* ***A****ccess* ***I****ntegration* (RAI) mode, which automatically adjusts the integration time from pixel to pixel based upon the real-time observation of photon flux using CID random accessibility and NDRO (see Figure 4). It is with this RAI mode that extended dynamic range (~10^6) can be achieved, and it is this mode that was used for the measurements presented here.

In RAI mode, the user defines a maximum exposure time and one or more regions of interest (ROI) defined with a horizontal origin (Xo), a vertical origin (Yo), a horizontal size (dX) and a vertical size (dY). The user may also define a desired 'binning' resolution (Xbin, Ybin). For example, a user could define an ROI as follows: Xo = 345, Yo = 128, dX = 15, dY = 3, Xbin = 1, and Ybin =3. (Note that for this beam profiling applications, the Xbin and Ybin values are set to 1 in order to maximize image resolution.) For

this example, whenever it is necessary for the algorithms to interrogate this ROI, 15 readings would be acquired with a 1 by 3 binning pattern starting at the ROI origin (Xo = 345, Yo = 128). In addition to the overall ROI, the user must also define a 'Control Region,' which is typically smaller than the overall ROI and includes the most intensely illuminated pixel. In the example listed here, the 'Control Region' could be a 3 by 3 pixel area in the middle of the ROI (Xo = 351, Yo = 128, dX = 3, and dY = 3). The RAI algorithms sequentially observe the 'Control Regions' for the user defined ROIs in a circular queue. Whenever the signal on the 'Control Region' reaches a threshold signal level (typically defined as 75% of full well capacity), the entire ROI is read, the data is stored in the camera RAM, and finally the pixels in the ROI are reset (injected) and a new integration cycle is begun. Each ROI is cycled as many times as necessary until the user defined maximum exposure time expires. These RAI algorithms dramatically extend dynamic range because the maximum observable signal is not limited by full well capacity, but rather it is limited by the number of times the ROI can be cycled given the user defined maximum exposure time. In many applications, the ROI can be cycled tens or hundreds of thousands of times in the user defined exposure period thereby extending dynamic range by 3 or 4 orders of magnitude.

There are limits to the RAI mode. The maximum cycle frequency of an ROI, which in turn limits the maximum achievable dynamic range, depends on numerous factors including: the total number of user defined ROIs in the RAI circular queue, the number of pixels in each ROI, whether or not binning is employed, camera readout frequency (either 50 kHz or 200 kHz with the SpectraCAM™84), and the illumination level on the user defined ROIs. For these beam profile experiments, the dynamic range could be further improved by disregarding the central region of the beam and simply limit the observations to the halo regions of the light distribution by defining ROIs only in those regions.

The first measurements with the SpectraCAM™84 camera were done with a Picoquant PDL 800-B laser. This laser provides additional intensity tuning capabilities in comparison to the aforementioned experimental setup. These additional tuning capabilities proved to be beneficial for the first operation and test of the camera.

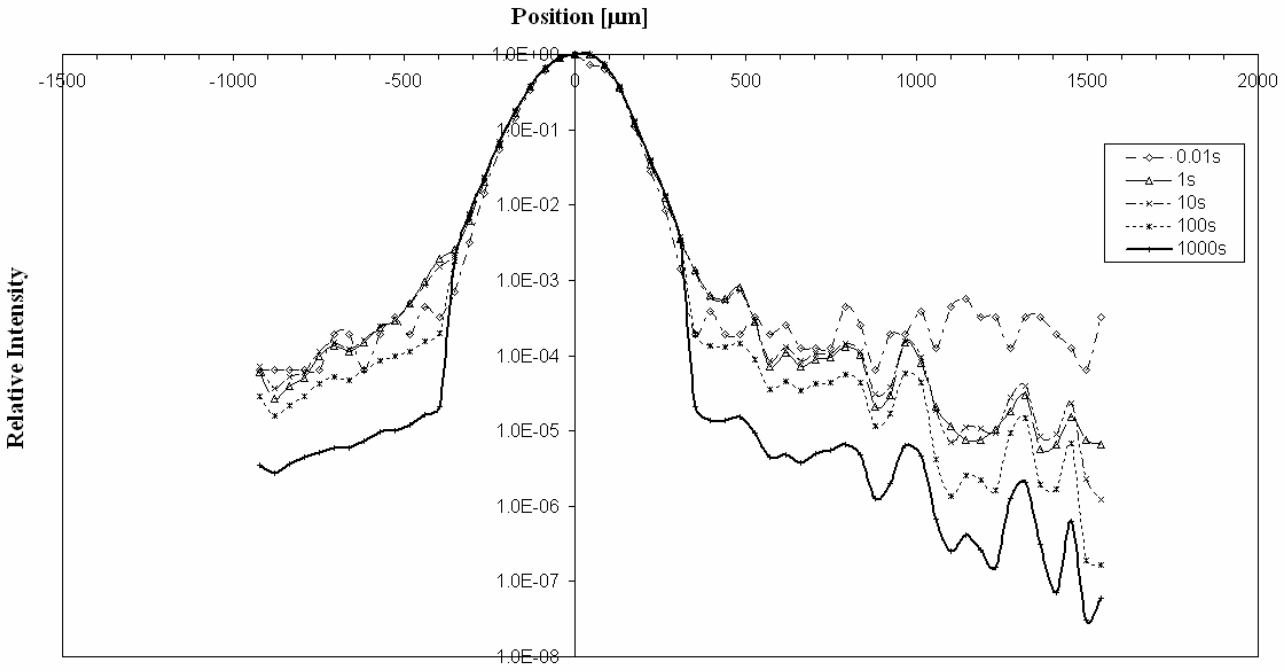

Figure 5: Normalized intensity distribution of the Picoquant PDL 800-B laser as measured with the CID camera with different acquisition times.

The measured intensity distribution as a function of position along one of the main axes and different maximum exposure times is shown in Figure 5. It can be clearly seen that the shape of the central, highly illuminated region is maintained independent of the maximum exposure time. In addition, the level of detail that can be measured in the tail regions of the light distribution can be greatly improved by using longer maximum exposure times. Signal-to-noise ratios of up to 10^7 can be observed in the case of a 1000 second measurement.

PHOTO MULTIPLIER SETUP

In order to have comparative data to the CID camera, a step-by-step measurement system with a photo multiplier tube mounted on a horizontal and vertical translation stage was developed and used to scan the same laser profile (see Figure 6).

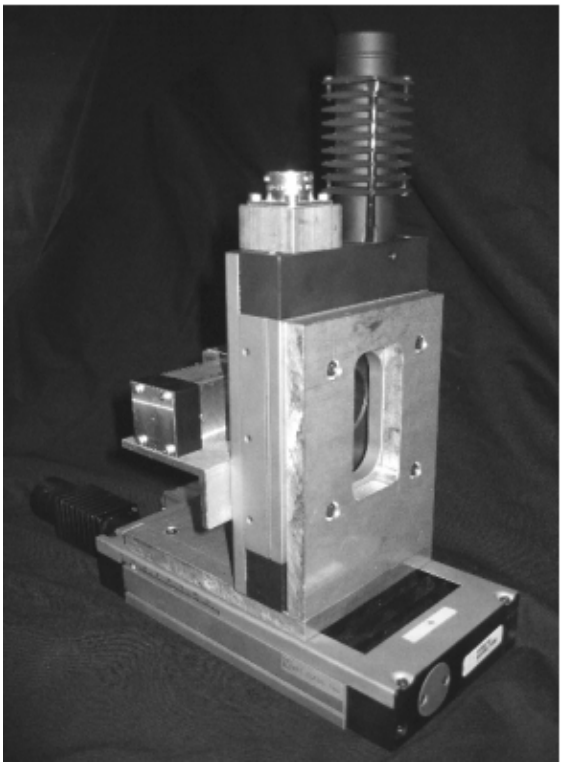

Figure 6: Photograph of the step-by-step PMT acquisition system

A Hamamatsu photomultiplier tube type R7400U [11] was installed into a small metallic mount, which included facilities to insert optical density filters whenever necessary. The diameter of the central aperture of the mask in front of the PMT could be varied from 0.5 mm to several millimetres, covering all possible beam dimensions. The step size for the measurements was 100 μm, and thus a deconvolution of the initial data was performed to ensure comparability to the other measurements. However, it should be mentioned that the size of the aperture still leads to a signal averaging aberration because the aperture is large in comparison to the absolute pixel sizes of both the CCD and the CID camera.

The results from these measurements are given in Figure 7. While the results for all three techniques are in substantial agreement in the central beam region, the maximum achievable dynamic range of the CCD camera is limited to about two orders of magnitude. The PMT setup clearly improves on that, covering five orders of magnitude. By choosing a different photomultiplier with a higher amplification of the signal and optimizing on the size and shape of the central aperture in the mask, one could possibly extend the dynamic range further with the PMT aparatus. For the envisaged measurements in CTF3, the demonstrated dynamic

range already covers the required signal levels. The PMT apparatus has been installed in the accelerator and will be tested in the near future.

The highest dynamic range, and best results, were achieved with the CID camera, where the maximum exposure time was set to ten minutes, which is a reasonable time from a practical point of view. Due to the limited dynamic range of the CCD on one hand, and the signal averaging aberration of the PMT setup on the other, the measurement with the CID camera showed a number of details that were not observable with the other two methods.

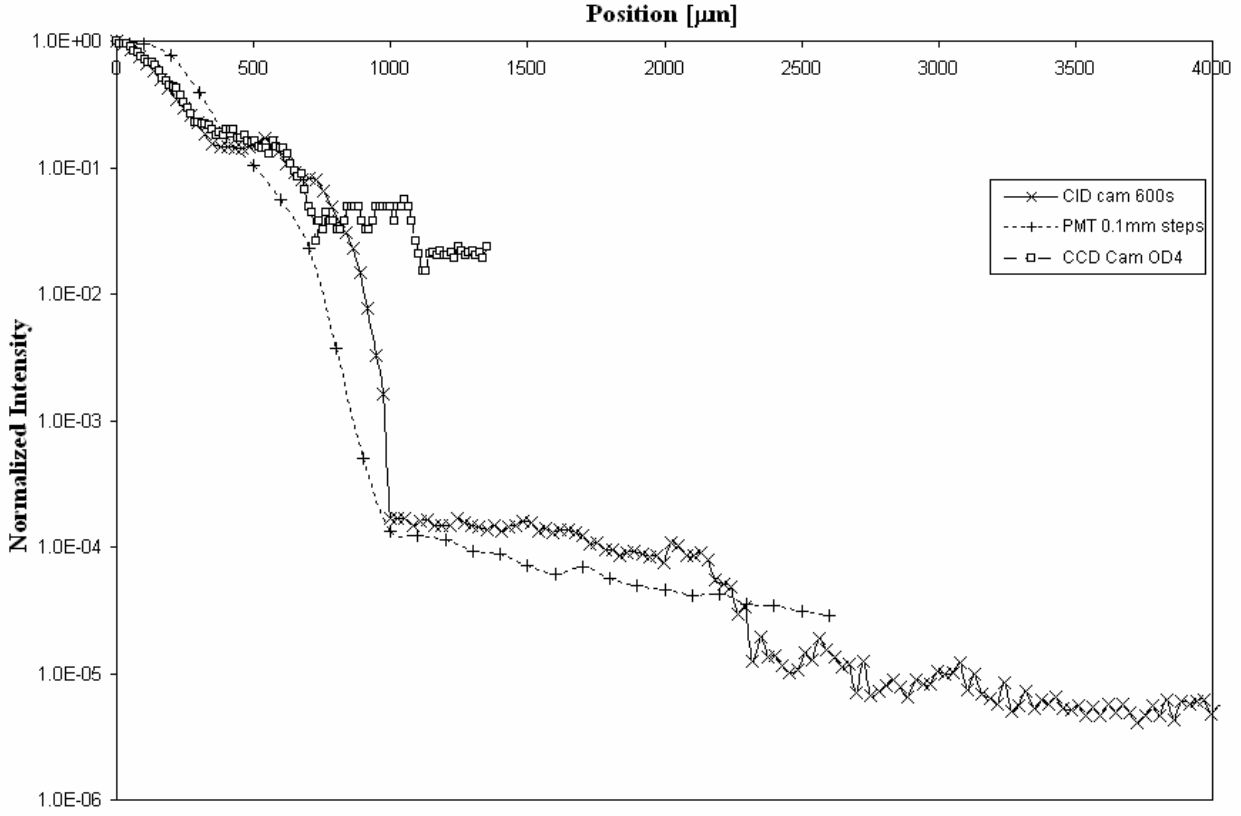

Figure 7: Measured normalized intensity as a function of position for the CCD and CID cameras and the step-by-step measurement with the photomultiplier

Besides the measurement with the pulsed laser, CID camera tests were made with other light sources confirming dynamic ranges 10^6 and beyond without special shielding of background light or the deployment of optical density filters. A comparison between the parameters of the three different acquisition methods is shown in Table 1. Concerning the CID camera system, it should be mentioned that the overall camera apparatus is not extremely radiation hard despite the inherent radiation resistance of the CID imager itself. Any such CID camera system installed in an environment like CTF3 must be appropriately shielded.

Table 1: Summary of the acquisition parameters of the three different systems

	CCD camera	**PMT setup**	**CID camera**
Pixel Size [μm]	6.5 x 6.25	100 x 100	27 x 27
Dynamic Range	10^2	10^5	10^6
Measurement Time [s]	1	~1800	600
Radiation hardness	Fair	Fair	Poor
Time resolution	~ ms	~ ns	> ms
Cost	$	$	$$

CONCLUSION

For a future understanding of beam halo formation and evolution in electron accelerators, it is not only necessary to have accurate models of the underlying mechanisms, but also it is necessary to have measurement techniques that are able to cover a dynamic range large enough to provide reasonable signals even in the beam tails. Optical techniques based on optical transition radiation provide an interesting approach to such measurements. While standard acquisition systems based on CCD technology are typically limited to dynamic ranges of 10^2 - 10^3, CID technology provides methods to cover dynamic ranges up to 10^6 and possibly even beyond. The CID technology offers the unique possibility to define regions of interest in real time during an RAI mode acquisition, thereby optimizing the dynamic range.

REFERENCES

[1] A.V. Fedotov, “Mechanisms of halo formation”, AIP Conf. Proc. **693** (3), 2003

[2] C.K.Allen et al., "Beam Halo Measurements in High-Current Proton Beams," Phys. Rev. Lett. **89** (214802), 2002

[3] T.P. Wangler, “Physics Results from the Los Alamos Beam-Halo Experiment”, AIP CP **693** (108), 2003

[4] J.S.O'Connell, T.P.Wangler, R.S.Mills, and K.R. Crandall," Beam Halo Formation From Space-Charge Dominated Beams in Uniform Focusing Channels", Proc. Part. Acc. Conf., IEEE Catalog No. CH3279-7, (3657-3659), 1993

[5] R.L. Gluckstern,"Analytic Model for Halo Formation in High Current Ion Linacs", Phys. Rev. Lett. **73** (1247), 1994

[6] T.P.Wangler, K.R.Crandall, R. Ryne, and T.S.Wang,"Particle-core model for transverse dynamics of beam halo", Phys.Rev. ST-AB **1** (084201), 1998

[7] L. Wartski, "Etude du rayonnement de transition optique produit par des électrons d'énergie 30 à 70 MeV. Application aux diagnostics de faisceaux de particules chargées.", Thesis at the Université de Paris-Sud (1976)

[8] T. Lefèvre et al, "Beam Halo Monitoring on the CLIC Test Facility 3", Proc. European Part. Acc. Conf., Lucerne, Switzerland, 2004

[9] http://www.vialux.de

[10] G. Michon, H. Burke, "Operational characteristics of CID imager", Solid-State Circuits Conference. Digest of Technical Papers. IEEE International Volume XVII (26) 1974

[11] http://www.hamamatsu.com